**Title**

# BTK operates a phospho-tyrosine switch to regulate NLRP3 inflammasome activity

**Authors**

Zsófia A. Bittner[a,§], Xiao Liu[a], Sabine Dickhöfer[a], Hubert Kalbacher[b], Karlotta Bosch[a], Liudmila Andreeva[c,d], Sangeetha Shankar[a], Ana Tapia-Abellán[a], Ana Marcu[a], Stefan Stevanovic[a], Matthew Mangan[e,f], Peter Düwell[e], Marta Lovotti[e], Franziska Herster[a], Markus W. Löffler[a,g,h,i] , Olaf-Oliver Wolz[a,$], Nadine A. Schilling[j], Jasmin Kümmerle-Deschner[k], Samuel Wagner[l], Anita Delor[m], Bodo Grimbacher[m,n,o,p,q], Hao Wu[c,d], Eicke Latz[e,r] , Alexander N. R. Weber[a,i]*

**Affiliations**

[a] Interfaculty Institute for Cell Biology, Department of Immunology, University of Tübingen, Auf der Morgenstelle 15, 72076 Tübingen, Germany

[b] Interfaculty Institute of Biochemistry, University of Tübingen, Hoppe-Seyler-Str. 4, 72076 Tübingen, Germany

[c] Department of Biological Chemistry and Molecular Pharmacology, Harvard Medical School, 240 Longwood Avenue, C-213, Boston, MA 02115, USA

[d] Program in Cellular and Molecular Medicine, Boston Children's Hospital, 3 Blackfan Circle, Boston, MA 02115, USA

[e] Institute of Innate Immunity, University Hospital Bonn, Sigmund-Freud-Str. 25, 53127 Bonn, Germany

[f] German Center for Neurodegenerative Diseases (DZNE), Bonn, Germany.

[g] Department of General, Visceral and Transplant Surgery, University Hospital Tübingen, Hoppe-Seyler-Str. 3, 72076 Tübingen, Germany

[h] Department of Clinical Pharmacology, University Hospital Tübingen, Auf der Morgenstelle 8, 72076 Tübingen, Germany

[i] iFIT – Cluster of Excellence (EXC 2180) "Image-Guided and Functionally Instructed Tumor Therapies", University of Tübingen, Germany

[j] Institute of Organic Chemistry, University of Tübingen, Auf der Morgenstelle 18, 72076 Tübingen, Germany

[k] Department of Pediatrics I, University Hospital Tübingen, Hoppe-Seyler-Str. 1, 72076 Tübingen, Germany

[l] Interfaculty Institute of Microbiology and Infection Medicine, University of Tübingen, Elfriede-Aulhorn-Str. 6, 72076 Tübingen, Germany

[m] Centre of Chronic Immunodeficiency, University Hospital Freiburg, Engesserstr. 4, 79108 Freiburg, Germany

[n] Institute for Immunodeficiency, Center for Chronic Immunodeficiency (CCI), Medical Center, Faculty of Medicine, Albert-Ludwigs-University of Freiburg, Germany

[o] DZIF – German Center for Infection Research, Satellite Center Freiburg, Germany

[p] CIBSS – Centre for Integrative Biological Signalling Studies, Albert-Ludwigs University, Freiburg, Germany

[q] RESIST – Cluster of Excellence 2155 to Hanover Medical School, Satellite Center Freiburg, Germany

[r] Division of Infectious Diseases & Immunology, University of Massachusetts, 364 Plantation St, Worcester, MA 01605, USA

**Contact information**

* to whom correspondence should be addressed: Alexander Weber; Interfaculty Institute for Cell Biology, Department of Immunology, University of Tübingen, Auf der Morgenstelle 15, 72076

Tübingen, Germany; Tel. +49 7071 2987623; Fax. +49 7071 294759; alexander.weber@uni.tuebingen.de

[$] Current address: CureVac AG, Paul-Ehrlich-Straße 15, 72076 Tübingen, Germany.

[§] Current address: Department of Biology, Institute of Molecular Health Sciences, ETH Zürich, Zürich, Switzerland

## Funding

The study was supported by the Else-Kröner-Fresenius Stiftung (to ANRW), the Deutsche Forschungsgemeinschaft (German Research Foundation, DFG) grants CRC TR156 “The skin as an immune sensor and effector organ – Orchestrating local and systemic immunity” (to ZSB, FH and ANRW) and We-4195/15-1 (to ANRW), University Hospital Tübingen (Fortüne Grant 2310-0-0 to XL and ANRW), IFM Therapeutics (to ANRW), the “E-rare” program of the European Union, managed by the DFG, grant code GR1617/14-1/iPAD (to BG), and the „Netzwerke Seltener Erkrankungen“ of the German Ministry of Education and Research (BMBF, GAIN_ 01GM1910A, to BG) and the Damon Runyon Cancer Research Foundation (to LA). Infrastructural funding was provided by the University of Tübingen, the University Hospital Tübingen and the DFG Clusters of Excellence "iFIT – Image-Guided and Functionally Instructed Tumor Therapies" (EXC 2180, to AW), “CMFI – Controlling Microbes to Fight Infection (EXC 2124, to AW), “CIBSS – Centre for Integrative Signalling Studies” (EXC 2189, to BG) and “RESIST – Resolving Infection Susceptibility” (EXC 2155, to BG). Gefördert durch die Deutsche Forschungsgemeinschaft (DFG) im Rahmen der Exzellenzstrategie des Bundes und der Länder - EXC 2180 (390900677), EXC 2124, EXC 2189 (390939984) and EXC 2155 (39087428).

## Abstract

Inflammation is required for host defense as well as wound healing but wields enormous destructive potential, highlighting the need for multiple 'checks and balances' (*1*). The NLRP3 inflammasome, a pivotal molecular machine for the maturation of IL-1 family pro-inflammatory cytokines (*1*), is controlled by accessory proteins (*2, 3*), post-translational modifications (*4, 5*), localization (*6, 7*) and oligomerization (*8*). How these factors act in concert is unclear. We show that the established drug target and NLRP3 regulator, Bruton's Tyrosine Kinase (BTK) (*2, 9*), integrates several levels of regulation to boost inflammasome activity: by directly phosphorylating four conserved tyrosine residues in the polybasic linker region of NLRP3, BTK weakens the interaction of NLRP3 with Golgi phospholipids and may thus guide NLRP3 localization. BTK activity also promotes NLRP3 oligomerization and subsequent formation of inflammasomes. As NLRP3 tyrosine modification impacts on IL-1β release, we propose a novel BTK- and charge-mediated molecular phospho-switch to contribute to NLRP3 regulation. Collectively, our study highlights BTK as a 'multi-layer regulator' of the inflammasome and NLRP3 multi-tyrosine phosphorylation as a therapeutic target for restricting excess inflammation.



## Keywords

NLRP3 inflammasome, Bruton's Tyrosine Kinase (BTK), Interleukin-1, Inflammation, Ibrutinib, Macrophage, X-linked agammaglobulinemia, Cryopyrin-associated periodic syndrome (CAPS).

## Introduction

Inflammation mediated via the NLRP3 inflammasome supports the resolution of infections and sterile insults but also contributes to pathology in multiple human diseases such as Cryopyrin-associated periodic fever syndromes (CAPS), gout, stroke or Alzheimer's disease, and atherosclerosis (*10, 11*). Thus, the activity of the NLRP3 inflammasome, a molecular machine maturing IL-1 family cytokines via the activity of caspase-1, is tightly controlled at several levels: At the structural level, recent cryo-EM studies demonstrated that the 3D conformation of NLRP3 is critical for NLRP3 oligomerization and may depend on ADP/ATP binding (*8*). In addition, NLRP3 binding proteins, such as NEK7, have been shown to have an impact on inflammasome activity (*3, 12*). Moreover, post-translational modifications of NLRP3 enhance or reduce its activity by only partially elucidated mechanisms (*5*). Finally, NLRP3 interacts dynamically with subcellular organelles such as the trans-Golgi network (TGN): Whilst a polybasic region in the linker connecting the NLRP3 pyrin (PYD) and NACHT domains appears to control phosphatidylinositol-4-phosphate (PtdIns4P)-dependent tethering of NLRP3 at the disperse TGN (*6*), dissociation from the TGN into the cytosol was proposed a requirement for the nucleation of larger NLRP3 oligomers and, subsequently, the assembly of the complete inflammasome complexes, including ASC and caspase-1 (*7*). The cues instigating this shift in localization are not well understood. How these multiple layers of NLRP3 regulation are related or even integrated at the cellular as well as at the molecular level remains unclear. If individual regulators were to provide this integration, they could be valuable targets to modulate inflammasome activity.

We and others have recently identified Bruton's tyrosine kinase (BTK) as a novel and therapeutically relevant NLRP3 regulator (*2, 13*), which is rapidly activated upon NLRP3 inflammasome stimulation, and interacts with NLRP3 and ASC in overexpression systems. Its genetic ablation led to reduced IL-1β secretion *in vitro* and, importantly, in human patients *ex vivo* (*2*). BTK is a well-known cancer target for which FDA-approved inhibitors such as ibrutinib exist (reviewed in Ref. (*9*)). Based on the

molecular mechanisms and chronic inflammatory processes observed in the pathology of many cancers, targeting NLRP3 via BTK also appears as an attractive therapeutic option in other diseases.

Here we report that BTK directly modifies NLRP3 at four tyrosine residues in the PYD-NACHT polybasic linker, affecting its ability to bind PI4P and localize at the Golgi. Consequently, ablation of BTK kinase activity or tyrosine mutation decreased the formation of NLRP3 oligomers and IL-1β release, respectively. Our data suggest that this BTK-mediated phospho-tyrosine switch affects the activity of NLRP3 by modifying the charge of the PYD-NACHT polybasic linker and, consequently, altering its subcellular localization. BTK thus emerges as an important regulation hub for the activation of the NLRP3 inflammasome at multiple levels.

## Results

### BTK deficiency coincides with reduced NLRP3 tyrosine phosphorylation

Based on previous work (*2*), we hypothesized that BTK and NLRP3 may engage in a direct kinase-substrate relationship, whose elucidation might unravel novel molecular aspects of NLRP3 inflammasome regulation. We sought to test this in *Btk*-deficient primary murine BMDMs and in PBMCs from patients with the genetic *BTK* deficiency, X-linked agammaglobulinemia (XLA). As expected, IL-1β release upon nigericin stimulation was significantly reduced in BTK-deficient BMDMs and patient-derived PBMC, respectively (Fig. 1A, B). Interestingly, in BMDMs, endogenous NLRP3 precipitated and interacted with endogenous BTK in WT but not *Btk* or *Nlrp3* KO BMDM (Fig. 1C), irrespective of the BTK kinase inhibitor ibrutinib. Similarly, BTK co-immunoprecipitated with NLRP3 in PBMCs from healthy donors (HDs) (Fig. 1D). Thus, in both human and murine primary immune cells BTK and NLRP3 interact constitutively and independently of nigericin stimulation. This was also confirmed with a cell-free *in vitro* pull-down of recombinant purified NLRP3 and BTK proteins (Fig. 1E, Ref. (*8*) and Methods). We next tested whether BTK is able to phosphorylate NLRP3 upon nigericin treatment. In murine BMDMs (Fig. 1F) immunoprecipitated NLRP3 became rapidly phospho-tyrosine (p-Y)-positive, in cells expressing Btk but not in *Btk* or *Nlrp3* KO cells. Similarly, NLRP3 phosphorylation was also observed in healthy donor PBMCs (Fig. 1G), and lower in XLA PBMCs (Fig.

S1A). Importantly, treatment with λ-phosphatase abolished p-Y reactivity, further confirming the phospho-antibody specificity. Thus, BTK and NLRP3 interact endogenously in primary immune cells and BTK promotes NLRP3 tyrosine-phosphorylation upon nigericin stimulation.

## BTK kinase activity is required for NLRP3 tyrosine phosphorylation

We next tested whether BTK kinase activity was required for NLRP3 tyrosine phosphorylation. Two independent cell-free *in vitro* setups showed that the presence of BTK was necessary and sufficient for NLRP3 p-Y modification (Figs. 1H and S1B). However, in both PBMC and the *in vitro* setup NLRP3 tyrosine phosphorylation was blocked by ibrutinib treatment (Figs. 1I and S1B) and, thus, dependent on BTK kinase activity. Next, HEK293T cells were transfected with NLRP3 and BTK, and treated with or without BTK inhibitors. NLRP3 and BTK interacted independently of BTK kinase inhibitors, ibrutinib and acalabrutinib; however, NLRP3 tyrosine phosphorylation was abrogated in the presence of both BTK kinase inhibitors (Fig. 1J), consistent with results in primary BMDM (*cf.* Fig. 1C). In contrast, the NLRP3-specific inhibitor, MCC950 (*14*), failed to prevent BTK-specific interaction and NLRP3 p-Y positivity (Fig. 1J). Interestingly, the expression of kinase-dead (KD) BTK (K430E mutation, see Ref. (*9*)) was not able to induce NLRP3 tyrosine phosphorylation, despite an intact interaction (Fig. 1K). Similar results were obtained in the *in vitro* cell-free setup (*cf.* Fig. S1B). Thus BTK kinase activity emerged as essential and sufficient for NLRP3 p-Y modification using primary immune cells, the HEK293T system or purified recombinant proteins, indicative of a direct kinase-substrate relationship.

## BTK phosphorylates four conserved tyrosine residues in the NLRP3 PYD-NACHT linker domain

To map the modified tyrosine residues in NLPR3, we compared Flag-tagged full-length with truncated NLRP3 constructs (*15*) of only the PYD (1-93), the extended NACHT domain (94-534), which includes an N-terminal linker domain (94-219) (*8*), and the LRR domain (535-1,036). BTK exclusively phosphorylated the NLRP3 extended NACHT construct (Fig. 2B, C), ruling out Y816 (*5*) as the phospho-site. Mutation of the nine tyrosines in the core NACHT domain (220-534, (Fig. 2D) to

phenylalanine (F) did not impact the level of phospho-NLRP3 detected upon BTK co-expression (Fig. S3A, quantified in S3B). However, when the linker (94-219) tyrosines were targeted (Fig. 2E), mutated Y168 showed partial but significant reduction of the p-Y signal, as shown by conventional immunoblotting (Fig. 2F, quantified in G) and WES capillary electrophoresis analysis (Fig. 2H, quantified in S3C), respectively. Thus, Y168 emerged as a novel putative phospho-tyrosine site in NLRP3, specifically modified by BTK. Unfortunately, the linker region is not accessible to mass spectrometric analysis (data from (*16*) plotted in Fig. S3D). Therefore, to assess the phosphorylation of Y168 by alternative means, 15-mer peptides covering all linker tyrosines (*cf.* Fig 2E and Table S1) were incubated with His-tagged BTK to assess peptide phosphorylation in a cell-free system. Following BTK removal by anti-His beads, p-Y phosphorylation of the peptides was visualized by dot blot analysis. While the majority of Y-containing peptides and all F-containing corresponding peptides were not phosphorylated (Fig. S3E), the Y168-containing peptide showed strong tyrosine modification (Fig. 2I). Of note, peptides containing Y136, Y140, or Y143 – either in combination or as single tyrosines – were also phosphorylated (Fig. 2I), similar to peptides containing the sequences in mouse NLRP3 (Y132, Y136, Y145 and Y164, see Fig. S3F). In HEK293T cells, combined mutations of Y136, Y140, Y143 ("3Y>F") and additionally Y168 to phenylalanine ("4Y>F") consequently led to a strong reduction of the p-Y signal, both in a FL-NLRP3 construct and when the linker was fused to an mCitrine yellow fluorescent protein-HA sequence (here termed 'hLinker-Cit-HA', Fig. 2J). Consistent with the only partial effect of a single Y168F mutation (*cf.* Fig. 2F-H), BTK appears able to specifically modify not only one, but at least four tyrosines – Y136, Y140, Y143 and Y168 – in the PYD-NACHT linker of human (and murine) NLRP3 *in vitro*.

To gain a structural insight, we mapped the sites in a recent cryo-EM structure of an NLRP3-NEK7 complex (Ref. (*8*), Fig. 2K and S4A). Interestingly, Y136, Y140 and Y143 were found in a helical region proposed to contact the PYD for ASC recruitment (*8*). Further, Y168, which maps to the vicinity of several likely pathogenic CAPS mutations (*cf.* Fig. S2), was adjacent to a putative ADP molecule and might thus influence nucleotide binding (Fig. 2L, M). Interestingly, all of the BTK-modified Y residues

were strongly conserved in other NLRP3 sequences, further highlighting their potential functional relevance (Fig. S4B). Collectively, our results suggest that BTK directly modifies multiple highly conserved tyrosines within a functionally important domain in NLRP3 that could impact downstream steps in the assembly of the oligomeric inflammasome complexes.

## BTK-mediated phosphorylation sites affect PI4P binding

Chen and Chen recently identified a 'polybasic' motif (K127-130 in mouse; K127 and K129-130 in human NLRP3) as critical for NLRP3 charge-dependent binding to Golgi phosphatidylinositol-4-phosphates (PI4Ps) and inflammasome nucleation (*6*). Unexpectedly, Y136, Y140 and Y143 precisely mapped to this polybasic motif in the NLRP3 PYD-NACHT linker, and interdigitate with the basic residues mediating the proposed NLRP3 interaction with negatively charged membrane phospholipids (Fig. 3A). The mutation of three positively charged residues (K127, K129, K130) in the mNLRP3 polybasic region to alanine (K>A) is sufficient to abrogate PI4P binding (*6*). We therefore hypothesized that BTK phosphorylation of Y136, Y140 and Y143 might weaken the proposed charge attraction of NLRP3 with Golgi PI4Ps. (*6, 7*). Charge computations suggested that at cytoplasmic pH 7.4, the net charge of the human NLRP3 polybasic linker sequence shifts from +7.28 (unphosphorylated) to +2.01 if Y136, Y140 and Y143 are phosphorylated in (Fig. 3B), and from +8.33 (unphosphorylated) to +3.06 (3x phosphorylated) for mouse NLRP3. To confirm this charge shift, synthetic phospho- and non-phospho versions of the Y136/Y140/Y143-containing peptides from both human and mouse NLRP3 were studied in pH titrations, demonstrating the phospho-Y-peptide to be significantly more acidic/negatively charged (Fig. 3C). Furthermore, in the NLRP3-NEK7 structure the 3x phospho-modification is calculated to cause a significant change in the computed surface charge of a 'hypothetically active' NLRP3 state (*8*) towards negative values (Fig. S5A). We therefore hypothesized tyrosine phosphorylation by BTK might weaken interactions with the negatively charged PI4Ps. Consistently, the binding of 4xY>E, i.e. phospho-mimetic, mutant human NLPR3 linker-Cit-HA fusion protein to PI4P beads (*6*) was reduced compared to the corresponding WT construct (Fig. 3D). This was further confirmed by the fusion of the murine NLRP3 polybasic region to

GFP-Flag (mPBR-GFP-Flag, construct as in Ref. (*6*)): Despite equal expression, the Y>E construct bound PI4P beads less strongly than WT (Fig. 3E). Reduced binding was also observed for the corresponding K>A mutant, which is known to be defective in PI4P binding based on charge neutralization (*6*). To test whether BTK activity might also affect Golgi localization, we fractionated different stimulated BMDM lysates into S100 (soluble, cytosol), P5 (heavy membrane, Golgi and mitochondria) and P100 (light membrane, ER and polysomes) fractions and probed them for NLRP3. BTK, whose PH domain also binds PIPs (references in (*17*), was also analyzed and found to localize similarly to NLRP3 (Fig. 3F, Fig. S5B), in keeping with earlier interaction analyses (*cf.* Fig. 1C, F). As expected (*6*), in both WT and *Btk* KO BMDMs, NLRP3 was detectable in the P5 fraction upon LPS treatment, indicating that BTK is not essential for initial NLRP3 localization *towards* P5 membranes (Fig. 3F, Fig. S5B). However, nigericin stimulation in WT BMDM coincided with progressive depletion of NLRP3 from the P5 fraction within 20 min, consistent with the timing of phosphorylation in these cells (*cf.* Fig 1F). Conversely, *Btk* KO BMDMs did not show dissociation within this time, suggesting NLRP3 interaction with Golgi membranes remain more stable in the absence of BTK, possibly due to intact charge-mediated PI4P-interactions (*6*). Collectively, these experiments show that both, the BTK-modified tyrosine positions in the NLRP3 linker and the presence of BTK, have an impact on NLRP3 linker-PI4P binding and subcellular fractionation of NLRP3; most probably via affecting linker charge (*cf.* Fig. 3A, C and S5A).

## BTK kinase activity affects NLRP3 oligomerization and IL-1β release

A recent study proposed that NLRP3 release from the Golgi was required for ASC engagement and full inflammasome assembly (*7*). As Golgi depletion was lower in the absence of BTK (*cf.* Fig. 3F), we explored whether BTK kinase activity also affected subsequent full inflammasome assembly, e.g. by recruiting ASC into complex formation. Indeed, native PAGE of nigericin-stimulated WT and *Btk* KO BMDM lysates (Fig. 4A) or BTK inhibitor- vs vehicle-treated *Pycard* (ASC) KO (Fig. 4B) showed reduced NLRP3 oligomers in BTK-deficient or –inhibited samples, and lower ASC cross-linking (Fig. 4C). Size exclusion chromatography of untreated WT cell lysates showed that BTK and NLRP3 co-eluted in the

high MW fraction (>1,100 KDa). Consistent with native PAGE in *Btk* KO or WT lysates from ibrutinib-treated cells, elution shifted to lower molecular weight complexes (Fig. 4D, E). Ablation of BTK activity, thus, appeared to reduce the subsequent ability of NLRP3 to oligomerize into large MW cytosolic inflammasomes and to assemble with ASC. To show that BTK-modified tyrosine residues - and the effects of BTK described so far - also had an impact on IL-1β release, NLRP3-deficient immortalized macrophages were retrovirally transduced with WT or tyrosine-mutated (4xY>F) NLRP3-T2A-mCherry constructs, allowing for cell sorting for equal protein expression (Fig. 4F). Compared to WT-transduced cells, cells with the 4xY>F construct failed to restore nigericin- and R837 (imiquimod)-dependent IL-1β release (Fig. 4G). Conversely, TNF release, which is NLRP3-independent (*2*), was comparable between cell lines (Fig. 4H). Likewise, IL-1β release upon stimulation with the NLRP3- and BTK-independent (*2*) AIM2 inflammasome stimulus, poly(dA:dT), was comparable between WT and mutant cells (Fig. 4G,H). The data show that the BTK-modified tyrosine positions identified here play an important role for full NLRP3 inflammasome activity and subsequent IL-1β release.

## Discussion

The mechanism of activation of the NLRP3 inflammasome has been intensely studied for some time and recent work has unraveled a critical role of the dynamic localization of NLRP3 at the Golgi in the regulation of its activity (*6*) (*7*). Using both biochemical and cellular assays in human and murine primary cells, we found that BTK directly participated in these processes at the level of NLRP3, providing novel molecular insights: direct phosphorylation of four conserved and functionally important tyrosine residues in the NLRP3 polybasic linker motif affected linker charge and phospho-mimetic mutation weakened NLRP3-PI4P interactions, presumably by neutralization of the linker net surface charge. In line with this, in the presence of BTK NLRP3 retention to the Golgi is seemingly less, NLRP3 inflammasome oligomerization, ASC association, and increased IL-1β secretion higher. Our data suggest that BTK-mediated phosphorylation of multiple NLRP3 tyrosines may serve as a molecular switch tuning NLRP3 charge and subsequently localization and inflammasome assembly. Modification, localization, and oligomerization of NLRP3 have been recognized to be important but, supposedly hierarchically separate layers of NLRP3 inflammasome regulation and, as consequence, of inflammation. Our data indicate that some of these layers may be integrated and interconnected by BTK: By decoding the most basal determinants such as protein sequence, BTK appears to integrate post-translational modification, surface charge, interaction with organelles, and ultimately assembly of a highly oligomeric molecular machinery (Fig. S6). Such a dense and interconnected network of regulation would be in line with the critical needs to tightly control excessive IL-1β release to prevent pathologies. Of course, other proteins also participate in this process and we cannot formally rule out effects of BTK at the level of ASC. Nevertheless, our data indicate that BTK is directly involved in licensing full IL-1β levels via the regulatory events characterized here. Furthermore, NLRP3 phosphorylation may represent a biomarker, and possibly therapeutic target, for early NLRP3 activation. Collectively, our work provides both a rationale as well as concrete targeting strategies that may be applied to block excess IL-1β production in acute inflammasome-related diseases.

## Abbreviations

AIM2 – Interferon-inducible protein absent in melanoma 2; ASC – Apoptosis-associated speck-like protein containing a Caspase activation and recruitment domain (CARD); BMDM – bone marrow-derived macrophages; BTK – Bruton's Tyrosine Kinase; FDA – Food and Drug Administration; CAPS – Cryopyrin-associated periodic syndrome; GM-CSF - Granulocyte-macrophage colony-stimulating factor; HD – healthy (blood) donor; HEK – human embryonic kidney; IFN – Interferon; IL – Interleukin; KD – kinase-dead; LPS – Lipopolysaccharide; LRR – leucine-rich repeat; NEK7 – NIMA related kinase 7; NACHT – NAIP, CIITA, HET-E and TEP1; NLR – Nod-like receptor; NLRP3 – NACHT, LRR and PYD domains-containing protein 3; PBMC - peripheral blood mononuclear cell; PH – Pleckstrin homology; PI4P – phosphatidylinositol-4-phosphate; PMA - Phorbol-12-myristate-13-acetate; p-Y – phospho-tyrosine; PYD – Pyrin domain; SH - Src homology; TGN – trans-Golgi network; TH - Tec homology; TLR – Toll-like receptor; TNF – Tumor necrosis factor; XLA - X-linked agammaglobulinemia.

## Materials and Methods

**Reagents.** Nigericin and Lipopolysaccharide (LPS) were purchased from Invivogen, ATP from Sigma, ibrutinib and acalabrutinib from Selleckchem, recombinant Granulocyte-macrophage colony-stimulating factor (GM-CSF) from Prepro-Tech, Ficoll from Merck Millipore. Peptides (EMC Microcollections Tübingen or synthesized in house) and antibodies are listed in Tables S1 and S2, respectively.

**Peptides.** Synthetic peptides were produced by standard 9-fluorenylmethyloxycarbonyl/tert-butyl strategy using peptide synthesizers P11 (Activotec, Cambridge, UK) or Liberty Blue (CEM, Kamp-Lintfort, Germany). Purity was assessed by reversed phase HPLC (e2695, Waters, Eschborn, Germany) and identity affirmed by nano-UHPLC (UltiMate 3000 RSLCnano) coupled online to a hybrid mass spectrometer (LTQ Orbitrap XL, both Thermo Fisher, Waltham, MA, USA). Lyophilized peptides were purified by standard HPLC. For certain peptides a pH titration with NaOH was performed using standard procedures. For *in vitro* assays peptides were dissolved at 10 mg/ml in dimethyl sulfoxide

(DMSO) and diluted 1:10 in bidestilled $H_2O$. Frozen aliquots were further diluted in cell culture medium and sterile filtered if necessary.

**Plasmid constructs.** ASC, NLRP3 and BTK coding sequences in pENTR clones were generated as described in (*18*). Truncated Flag-tagged NLRP3 constructs were a kind gift of F. Martinon, Lausanne, Switzerland (*15*). Constructs for the human PYD-NACHT linker (residues 94-219) fused to mCitrine-HA or the murine polybasic motif (residues 127-146) in the context of Flag-GFP (as in (*6*)) were synthesized by GeneWiz. Point mutations in BTK and NLRP3 were subsequently introduced using QuikChange II Site-Directed Mutagenesis Kit from Agilent Technologies, following the manufacturer´s instructions. Presence of the desired mutation and absence of unwanted regions in the entire CDS was confirmed by automated DNA sequencing.

**Study subjects and blood sample acquisition.** CAPS patients were recruited at the Department of Pediatrics, University Hospital Tübingen and XLA patients at the Centre of Chronic Immunodeficiency, University Hospital Freiburg, healthy blood donors at the Interfaculty Institute of Cell Biology, Department of Immunology, University of Tübingen. All patients and healthy blood donors included in this study provided their written informed consent before study participation. Approval for use of their biomaterials was obtained by the respective local ethics committees, in accordance with the principles laid down in the Declaration of Helsinki as well as applicable laws and regulations. XLA patients were clinically identified and genetically characterized as described in (*2*).

**Mice.** *Btk* KO (*19*) and *NLRP3* KO (Jackson stock No: 021302) and wild type C57BL/6J (Jackson) colonies were maintained in specific-pathogen free conditions under regular hygiene monitoring. All animal experiments were approved by local authorities and performed in accordance with local institutional guidelines and animal protection laws, including specific locally approved protocols for sacrificing.

**Cell culture.** All cells were cultured at 37 °C and 5% $CO_2$ in DMEM or RPMI supplemented with 10% fetal calf serum, L-glutamine (2 mM), penicillin (100 U/ml), streptomycin (100 µg/ml) (all from

Thermo Fisher). They were free of mycoplasma contamination and monitored regularly using a PCR-based assay.

**Isolation and stimulation of primary human immune cells.** Peripheral blood mononuclear cells (PBMCs) from healthy donors and patients were isolated from whole blood using Ficoll density gradient purification, primed with 10 ng/ml LPS for 3 h, and in some cases treated with 60 µM ibrutinib before stimulation with 15 µM nigericin for the indicated periods of time.

**Isolation of primary bone marrow-derived macrophages (BMDMs).** Bone marrow (BM) cells were isolated from femurs and tibiae of 8-12 week old mice, grown and differentiated using GM-CSF (M1 polarization) as described (*2*).

**Expression and purification of recombinant BTK, NEK7 and NLRP3.** The plasmids encoding NLRP3 with the deleted pyrin domain (amino acids 134–1034) for MBP-fusion protein expression in Bac-to-Bac system (Thermo Fisher) and human NEK7 for His-SUMO fusion protein expression in *E. coli* BL21 (DE3) were described recently (*8*). For NLRP3 expression the baculovirus of NLRP3 was prepared using the Bac-to-Bac system (Thermo Fisher). Protein expression was induced by infection of Sf9 cells with 1% v/v of baculovirus. 48 h after infection cells were lysed by sonication in buffer containing 30 mM HEPES, 200 mM NaCl, 2 mM 2-mercaptoethanol and 10% glycerol at pH 7.5 with freshly added protease inhibitor cocktail (Sigma). The supernatant was incubated with 3 ml amylose resin at 4°C for 1 h and subjected to gravity flow. NLRP3 protein was eluted with 50 mM maltose and further purified with size-exclusion chromatography on Superose 6 10/300 GL column (GE Healthcare) equilibrated with buffer containing 30 mM HEPES, 150 mM NaCl and 2 mM β-mercaptoethanol at pH 7.5. NEK7 was overexpressed in *E. coli* BL21 (DE3) overnight at 18 °C after induction with 0.1 mM isopropyl-β-d-thio-galacto-pyranoside after optical density at 600 nm reached 0.8. Cells were lysed by sonication in buffer containing 50 mM HEPES, 500 mM NaCl, 5 mM $MgCl_2$, 10 mM imidazole, 10% glycerol and 2 mM β-mercaptoethanol at pH 7.5 with freshly added protease inhibitor cocktail (Sigma). The His-SUMO-fusion NEK7 was purified by affinity chromatography using Ni-NTA beads (Qiagen) followed by size-exclusion chromatography on Superdex 200 10/300 GL column (GE Healthcare) equilibrated with

buffer containing 30 mM HEPES, 150 mM NaCl and 2 mM β-mercaptoethanol at pH 7.5. WT and kinase-dead mutant BTK were overexpressed in Expi293 cells (Thermo Fisher) using transient transfection with poly-ethylenimine 25K (Polysciences). Cells were harvested 96 h post transfection and lysed in buffer containing 50 mM HEPES, 150 mM NaCl, 2 mM 2-mercaptoethanol and 10% glycerol at pH 7.5 with freshly added protease inhibitor cocktail (Sigma). The FLAG-fusion proteins were subjected to affinity chromatography using anti-FLAG M2 affinity gel (Millipore Sigma), eluted with 3xFLAG-peptide (Millipore Sigma) and further purified by size-exclusion chromatography on Superdex 200 10/300 GL column (GE Healthcare) equilibrated with buffer containing 30 mM HEPES, 150 mM NaCl and 2 mM β-mercaptoethanol at pH 7.5. Proteins were concentrated to 2-7mg/ml, flash-frozen in liquid nitrogen and stored at -80 °C.

**In vitro pull-downs.** MBP-tagged NLRP3 (2 µM) was mixed with 4 µM His-SUMO-NEK7 or wild type or mutant FLAG-BTK in buffer containing 30 mM HEPES, 150 mM NaCl and 2 mM β-mercaptoethanol at pH 7.5, and incubated for 30 min at 30°C. The mixture was further incubated for 1 h with 40 µl amylose resin and washed twice with 500 µl of the same buffer, followed by 1 h elution with 50 mM maltose. 30% and 70% of the sample was loaded as input and elution fractions, respectively, and analyzed by SDS–PAGE and immunoblot using monoclonal Anti-Flag® M2-Peroxidase (HRP) or anti-p-Y antibody (Sigma-Aldrich).

**ELISA.** Human and murine IL-1ß, IL-6 or TNF in supernatants were determined by ELISA using half-area plates using kits by R&D Systems and Biolegend, determining triplicate points on a standard plate reader.

**Co-immunoprecipitation and immunoblot.** PBMCs or BMDMs were primed with LPS and stimulated with nigericin, washed with cold PBS and immediately lysed in RIPA lysis buffer containing protease/phosphatase inhibitors (Roche). A sample of the cleared lysate was taken before addition of the primary antibody (see Table S2). After 18 hours of rotation in the cold room, magnetic bead coupled secondary antibody (Protein G Dynabeads, Thermo Fisher) was added for another 90 min. The beads were then washed three times with lysis buffer, resuspended in SDS loading buffer and

boiled. HEK293T were transfected using $CaPO_4$ and lysed 48 hours later in RIPA buffer with protease/phosphatase inhibitors (Roche). Cleared lysates were subjected to immunoprecipitation of the NLRP3-HA or NACHT-FLAG fusion protein with Dynabeads (Sigma-Aldrich), or with agarose beads covered with PI4P (P-B004a, Echelon Biosciences). Washed beads were boiled in loading buffer and applied to standard SDS-PAGE on Thermo Fisher pre-cast gels, followed by immunoblot according to the antibody manufacturer's instructions. Membranes were exposed using Peqlab Fusion FL camera and FusionCapt Advance software. Quantification was conducted using the same software.

**WES capillary electrophoresis.** 3 µl of the prepared Western Blot lysates were run on ProteinSimple WES instrument according to the manufacturer´s instructions. Data were analyzed with the Compass for SW software comparing the p-NLRP3 signal with the heavy chain signal from the same run as an internal control.

**Native PAGE.** BMDMs were stimulated and lysed in RIPA lysis buffer without SDS: Lysates were centrifuged at 2,300 x *g* for 10 min to pellet DNA. Supernatant was centrifuged at 16,100 x *g* for 25 min and the pellet was resuspended in Native PAGE sample buffer (Thermo Fisher). The samples were loaded onto NuPage 3-8% Tris-Acetate gels (Thermo Fisher) without boiling and native PAGE was conducted using Tris-Glycine running buffer (Thermo Fisher). The gel was soaked in 10% SDS solution for 10 min before performing semi-dry transfer and continuing with conventional immunoblot.

**Crosslinking of ASC oligomers.** BMDMs were primed with LPS and treated with ibrutinib and nigericin. Cells were lysed in RIPA lysis buffer and pellets were cross-linked using DSS and analyzed as described in (*20*).

**Size exclusion chromatography.** BMDMs were stimulated and lysed in 50 mM Tris-HCl pH 7.4, 1% NP-40, and 150 mM NaCl. 100 µl cleared lysate were loaded on a Superdex 200 Increase 10/300 GL (GE Healthcare) column and proteins were eluted using ÄKTA Purifier (GE Healthcare) and buffer 50

mM Tris-HCL pH 7.4 and 150 mM NaCl with 0.25 ml/min flow. 200 µl fractions were collected and analyzed via Western-Blot.

**In vitro kinase assay**. For results in Fig. 1H, recombinant NLRP3 from Novus Biologicals **(**H00114548-P01) and BTK from Sino Biological (10578-H08B) or Abcam (ab205800) were incubated at 30 °C for 3 hours using CST kinase buffer (#9802) in the presence of 2 mM ATP. As a negative control, recombinant Posi-Tag Epitope Tag Protein (Biolegend) was used. Before and after kinase assay samples were boiled and analyzed via SDS PAGE and Western Blot. For results in Fig. S1B, NLRP3 and BTK (WT or KD) were purified as described above. For reaction 2 µM MBP-tagged NLRP3 was mixed with or without 0.2 µM purified FLAG-tagged BTK in buffer containing 30 mM HEPES, 150 mM NaCl, 12.5 mM $MgCl_2$, 2.5 mM ATP and 2 mM β-mercaptoethanol at pH 7.5 in presence or absence of ibrutinib (Selleckchem, cat. S2680). The mixture was incubated at 30°C and equal aliquots were taken at indicated time points. Samples were analyzed by SDS–PAGE and immunoblot using anti-p-Y antibody (Cell signaling, cat. 8954S).

**Dot blot analysis.** Synthetized peptides were incubated with recombinant BTK (Sino Biologicals) for 3 h in CST kinase buffer (#9802) supplemented with 2 mM ATP. Next, the samples were boiled and anti-His magnetic beads (Dynabeads™ His-Tag Isolation and Pulldown, Thermo Fisher) were added to deplete the samples of phosphorylated BTK. The samples were cleared from the magnetic beads and the supernatants were manually spotted on a nitrocellulose membrane. The dried spots were stained using the Pierce reversible protein stain to visualize total peptide amounts. Then the membrane was blocked with 5% BSA in TBS-T and conventional anti-phospho-Tyrosine primary and secondary antibody incubation steps followed.

**Subcellular fractionation.** Cells were homogenized using a 10 ml syringe and 27 G x 19 mm needles in homogenization buffer (0.25 M sucrose, 10 mM Tris HCl (pH 7.5), 10 mM KCl, 1.5 mM $MgCl_2$, protease inhibitor (Roche) and PhosStop (Roche)). Homogenized cells were centrifuged at 1,000 x *g* for 5 min to remove the nucleus. The supernatant was centrifuged at 5,000 x *g* for 10 min to obtain a

heavy membrane fraction (pellet, P5). The supernatant was centrifuged 100,000 x *g* for 20 min to separate a light membrane fraction (S100) from the cytosol. P5 and S100 were washed once with homogenization buffer and then used for sucrose gradient ultracentrifugation, separately. For sucrose gradient ultracentrifugation, a continuous 15-45% (w/w) sucrose gradient was prepared in 10 mM Tris-HCl (pH 7.5), 20 mM KCl, and 3 mM $MgCl_2$) using a Biocomp Gradient Station (Biocomp Instruments, Fredricton, NB, Canada). P5 or S100 was loaded on top of the gradient and centrifuged at 170,000 x *g* for 3 h. The gradient was fractionated into 12 fractions of 1.1 ml using the fraction collector module of a Biocomp Gradient Station.

**PI4P bead binding assays**. HEK293T cells were transfected with HA-tagged human WT or Y>E PYD/NACHT linker (residues 94-219)-mCitrine-HA constructs. Cells were lysed in RIPA buffer and PI4P (Echelon Biosciences, P-B004A) or the same amount of control beads (Echelon Biosciences, P-B000) were added to cleared lysates and incubated for 1.5 h on 4 °C while rotating. Beads were then washed 3 times with RIPA buffer, boiled and bound proteins were analyzed via immunoblot. Alternatively, cells were transfected with WT, Y>E or K>A Flag-tagged murine polybasic region (residues 127-146)-GFP-Flag constructs, adopted from (*6*). PI4P beads or control beads were blocked beforehand in 2% BSA, 0.5% NP-40 and 200 µg/ml Flag peptide (Sigma-Aldrich, F3290) for 2 h at 4°C. Transfected cells were then lysed in RIPA buffer and the expressed proteins were purified using Anti-FLAG® M2 Magnetic Beads (M8823, Merck). Beads were washed 3x with RIPA buffer and boiled to elute the purified polybasic region. Blocked PI4P beads or the same amount of control beads were added to the eluted protein, and incubated for 1.5 h on 4°C while rotating. Beads were then washed 3x8 min with RIPA buffer, resuspended in LDS sample buffer, boiled, and bound protein was analyzed using immunoblot.

**Reconstitution and analysis of NLRP3-deficient immortalized macrophages.** NLRP3-deficient immortalized macrophages (*21*) were retrovirally transduced with NLRP3 (WT or 4xY>F)-Flag-T2A-mCherry constructs as described in (*21*) and subsequently sorted for similar expression of mCherry. Similar NLRP3 expression was confirmed by anti-Flag immunoblot of cell lysates. Cells were seeded at

458 1x10$^5$ cells/well in a 96 well plate in 100ul, primed with LPS (200 ng/ml) for 3h and inflammasome
459 stimuli in optiMEM added as follows: nigericin at 8 µM for 1.5 h, R837 (imiquimod) at 20 µg/ml for 2
460 h or poly(dA:dT) at 200 ng per well with 0.5 µl lipofectamine 2000 for 4 h. IL-1β and TNF were
461 subsequently determined by IL-1β and TNF HTRF assay respectively (Cisbio; 62MIL1BPEH and
462 62MTNFAPEG).

463 **NLRP3 sequence analysis, structure inspection and charge prediction.** NLR sequences were
464 retrieved from UniProt and ClustalW aligned within Geneious R6 software. A hypothetical active
465 conformation of NLRP3 was modeled based on NLRP3-NEK7 structure in an inactive state (PDB 6NPY)
466 (*8*). NACHT domain reorganization and hypothetical NLRP3 oligomerization was generated, based on
467 the NLRC4 oligomer (PDB 3JBL) as a homology model template by introduction of a 90° rotation of
468 NBD-HD1 module (*8*). Phosphorylation of tyrosine residues of interest was performed in Pymol
469 (Schrödinger) using the PyTMs plugin (*22*). Electrostatic potential of the solvent accessible surface of
470 phosphorylated and non-phosphorylated NLRP3 models was calculated with PBEQ-Solver online
471 visualization tool (http://www.charmm-gui.org (*23-25*) and visualized with Pymol. Protein net
472 charges of the Y136, Y140 and Y143-containing linker were conducted with ProtPi (www.protpi.ch).

473 **Statistics.** Experimental data was analyzed using Excel 2010 (Microsoft) and/or GraphPad Prism 6, 7
474 or 8, microscopy data with ImageJ/Fiji, flow cytometry data with FlowJo 10. Normal distribution in
475 each group was always tested using the Shapiro-Wilk test first for the subsequent choice of a
476 parametric (ANOVA, Student's *t*-test) or non-parametric (e.g. Friedman, Mann-Whitney U or
477 Wilcoxon) test. p-values (α=0.05) were then calculated and multiple testing was corrected for in
478 Prism, as indicated in the figure legends. Values <0.05 were generally considered as statistically
479 significant and denoted by * throughout. Comparisons were made to unstimulated control, unless
480 indicated otherwise, denoted by brackets.

## Figure Captions

**Figure 1: NLRP3 directly interacts and is tyrosine phosphorylated by BTK.** (A, B) IL-1β release (triplicate ELISA) from WT vs *Btk* KO BMDM (A, n=5 each) or XLA vs healthy donor (HD) PBMCs (B, n=3-6). (C, D) Co-IP of NLRP3 from WT, *Btk* KO or *Nlrp3* KO BMDM (n=3) or ibrutinib-treated PBMC lysates (n=2). (E) *In vitro* pulldown of FLAG-tagged BTK or His-SUMO-tagged NEK7 by MBP-tagged NLRP3 (n=3). (F, G) as in C and D, respectively, but with anti-phospho-tyrosine (p-Y) IP (n=3 or 5, respectively). (H) as in E but using two different commercial suppliers, A and B, of recombinant BTK. PosiTag = specificity control. (I) as in G but with ibrutinib pre-treatment (n=2). (J, K) IPs from HEK293T cells transfected with NLRP3 and BTK WT or kinase dead (KD) constructs, or treated with inhibitors (n=2 each). A and B represent combined data (mean+SD) from 'n' biological replicates (each dot represents one mouse or patient/HD). C-K are representative of 'n' biological (HD or mouse) or technical replicates. * $p<0.05$ using Student's *t*-test (A) or one-way ANOVA with Dunnett´s correction (B).

**Figure 2: BTK phosphorylates the PYD-NACHT linker.** (A) NLRP3 domains (UniProt ID Q96P20). (B) IP from HEK293T cells transfected with NLRP3 and BTK constructs (n=3). (C) as in B but including ibrutinib (n=3). (D) Positions of targeted tyrosine residues. (E) Linker region including polybasic motif. (F) as in B but using Y to F point mutants and WT or kinase-dead (KD) BTK plasmids (n=4). (G) Quantification of F. (H) WES capillary electrophoresis of IP p-NLRP3 (n=3). (I) Dot blot of BTK kinase assay with 15-mer synthetic peptides (n=3). (J) as in F but also NLRP3 linker (WT or Y-mutated) fused to mCitrine-HA (n=3). (K) Tyrosines (red) highlighted in model of NLRP3 (blue)-NEK7 (yellow) complex (pdb: 6NPY). Close up view on dimer interface (L) and putative nucleotide binding site (M). G represents combined data (mean+SD) from 'n' biological replicates (each dot represents one replicate). B, C, F, H-J are representative of 'n' technical replicates. * $p<0.05$ according to one sample *t*-test (G).

**Figure 3: BTK phosphorylation of the NLRP3 polybasic motif enables Golgi/PI4P dissociation.** (A, B) Charge distribution (A) and ProtPi net charge computation (B) of unmodified and 3x phospho-peptide

polybasic human NLRP3 linker. (C) pH titration of peptides encompassing the polybasic motifs of human or murine NLRP3 as phospho- (blue) or non-phosphorylated control (red) peptide (n=3). (D) NLRP3 linker-Cit-HA constructs precipitated with PI4P beads (n=3). (E) as in D but murine NLRP3 polybasic region fused to GFP-HA (mPBR-GFP-HA, n=3). (F) Subcellular fractionation of nigericin-treated WT or *Btk* KO BMDM lysates (n=3). C represents combined data (mean+SD) from 'n' biological replicates. In D-E one representative example of 'n' technical replicates is shown. * $p<0.05$ according to two-way ANOVA (C).

**Figure 4: BTK modification affects NLRP3 oligomerization and IL-1β release.** (A-C) WT, *Btk* KO, *Nlrp3* KO or *Pycard* (ASC) KO BMDM stimulated and respective lysates analyzed directly by native PAGE (A, n=2 and B, n=4) or ASC cross-linked in the pellet (C, n=4) and/or analyzed by SDS-PAGE. (D) as in A but size exclusion chromatography (SEC) fractions (n=3). (E) as in D comparing inhibitor treated WT BMDM or *Btk* KO BMDM lysates (n=3). (F-H) NLRP3 expression levels (F), IL-1β (G) or TNF (H) release from WT or 4xY>F NLRP3-reconstituted NLRP3-deficient iMacs (n=3). G-H represent combined data (mean+SD) from 'n' technical replicates. A-F are representative of 'n' biological (mice) or technical replicates. * $p<0.05$ according to one-way ANOVA (H) or ANOVA with Sidak correction (G).

## Author contributions

ZAB, XL, SD, HK, KB, LA, AM, MM, PD, ML, FH, SS, ATA, OOW, NAS, SW and ANRW performed experiments; ZAB, XL, SD, HK, LA, SS, ML, MM, PD, FH, NAS, SW and ANRW analyzed data; MWL, JKD, AD and BG were involved in patient recruitment and sample acquisition; ZAB and ANRW wrote the manuscript and LA, PD, MWL, SS, ATA, SW, HW and EL provided valuable comments. All authors approved the final manuscript. ANRW and ZAB conceived and coordinated the study. *S.D.G.*

## Acknowledgements

We gratefully acknowledge Ulrich Wulle for help with peptide synthesis and Yamel Cardona Gloria for helpful comments. We thank Xiaowu Zhang and Felix Meissner for helpful advice on kinase target

532 residue identification and mass spectrometry, respectively. We thank all study subjects and their

533 families for participating in the study.

## References


1. M. S. J. Mangan *et al.*, *Nat Rev Drug Discov* **17**, 588 (Aug, 2018).
2. X. Liu *et al.*, *J Allergy Clin Immunol*, (Feb 16, 2017).
3. Y. He, M. Y. Zeng, D. Yang, B. Motro, G. Nunez, *Nature* **530**, 354 (Feb 18, 2016).
4. B. F. Py, M. S. Kim, H. Vakifahmetoglu-Norberg, J. Yuan, *Mol Cell* **49**, 331 (Jan 24, 2013).
5. N. Song, T. Li, *Front Immunol* **9**, 2305 (2018).
6. J. Chen, Z. J. Chen, *Nature* **564**, 71 (Dec, 2018).
7. Z. Zhang *et al.*, *J Exp Med* **214**, 2671 (Sep 4, 2017).
8. H. Sharif *et al.*, *Nature* **570**, 338 (Jun, 2019).
9. A. N. R. Weber *et al.*, *Front Immunol* **8**, 1454 (2017).
10. P. Duewell *et al.*, *Nature* **464**, 1357 (Apr 29, 2010).
11. L. Broderick, D. De Nardo, B. S. Franklin, H. M. Hoffman, E. Latz, *Annu Rev Pathol* **10**, 395 (2015).
12. J. L. Schmid-Burgk *et al.*, *J Biol Chem* **291**, 103 (Jan 1, 2016).
13. M. Ito *et al.*, *Nat Commun* **6**, 7360 (2015).
14. A. Tapia-Abellan *et al.*, *Nat Chem Biol* **15**, 560 (Jun, 2019).
15. A. Mayor, F. Martinon, T. De Smedt, V. Petrilli, J. Tschopp, *Nat Immunol* **8**, 497 (May, 2007).
16. A. Stutz, G. L. Horvath, B. G. Monks, E. Latz, *Methods Mol Biol* **1040**, 91 (2013).
17. Z. Li *et al.*, *Proc Natl Acad Sci U S A* **94**, 13820 (Dec 9, 1997).
18. H. Wang *et al.*, *Hepatology* **62**, 1375 (2015).
19. W. N. Khan *et al.*, *Immunity* **3**, 283 (Sep, 1995).
20. S. Khare, A. D. Radian, A. Dorfleutner, C. Stehlik, *Methods Mol Biol* **1417**, 131 (2016).
21. V. Hornung *et al.*, *Nat Immunol* **9**, 847 (Aug, 2008).
22. A. Warnecke, T. Sandalova, A. Achour, R. A. Harris, *BMC Bioinformatics* **15**, 370 (Nov 28, 2014).
23. A. D. MacKerell, *Abstr Pap Am Chem S* **216**, U696 (Aug 23, 1998).
24. S. Jo, T. Kim, V. G. Iyer, W. Im, *J Comput Chem* **29**, 1859 (Aug, 2008).
25. S. Jo, M. Vargyas, J. Vasko-Szedlar, B. Roux, W. Im, *Nucleic Acids Res* **36**, W270 (Jul 1, 2008).

**Title and Authors**

# BTK operates a phospho-tyrosine switch to regulate NLRP3 inflammasome activity

by Bittner *et al.*

## Supplemental figure legends

**Figure S1:** (A) Co-IP of NLRP3 from healthy donor (HD) or XLA patient PBMC lysates (n=3). (B) p-NLRP3 occurrence in the *in vitro* kinase assay with BTK or kinase-dead BTK (KD) upon incubation with ATP for the indicated periods of time, with and without inclusion of ibrutinib. (C) HEK293T cells were transfected with the indicated NLRP3 and BTK WT or mutant constructs, treated with inhibitors and lysates subjected to HA-IP and immunoblot (n=3 each). In A-C one representative of 'n' biological replicates is shown.

**Figure S2:** Annotation of NLRP3 sequence (UniProt ID Q96P20).

**Figure S3:** (A) Position of all mutated Tyr residues in Linker-NACHT construct. (B) Phosphorylation analysis of core-NACHT tyrosine NLRP3 mutants. HEK293T cells were transfected with the indicated NLRP3 mutant constructs and a BTK WT construct as indicated and lysates subjected to HA-IP and immunoblot as indicated (n=4 each). (B) Quantification of A combined from n=4 experiments. (C) Quantification of WES capillary electrophoresis of NLRP3 p-Y IPs from HEK293T cells (Fig. 2H) from n=3 experiments. (D) Mass spectrometric analysis of purified mNLRP3, digested with different proteases, showing combined (upper) and separate coverage (lower) information (Ref. (*16*)). (E) Dot blot of *in vitro* kinase assay of His-BTK and 15-mer synthetic peptides derived from human NLRP3 containing the indicated tyrosines stained with a total protein stain (upper; input) or anti-p-Y Abs (lower grid, n=3). (F) As in E but with peptides derived from murine NLRP3 (n=3). B, D represent combined data (mean+SD) from 'n' biological replicates. In E-F one representative of 'n' biological replicates is shown. * $p<0.05$ according to one sample *t*-test (B, C).

**Figure S4:** Structural aspects and conservation of BTK-modified tyrosine residues in NLRP3. (A) NLRP3 model 6NPY showing NLRP3 Linker-NACHT-LRR (blue) and NEK7 C-terminal lobe (yellow). A putative bound ADP molecule and selected tyrosines are highlighted. (B) ClustalW multiple sequence alignments of NLRP3 sequences from other species. Coloring according to similarity (black = conserved). BTK-modified tyrosines are highlighted (residue numbering according to human NLRP3).

**Figure S5:** (A) CHARMM surface charge predictions of Linker-NACHT-LRR structure in the non-phosphorylated (left) and 4x phosphorylated (right) form. Blue = positive, red = negative charge. Grey boxes indicate that the area of charge alterations in the monomers maps to a contact area in the hypothetical dimer (center, rotated by 90 °; see relative position in oligomer, below). (B) Sucrose gradient fractionation of WT and *Btk* KO BMDM lysates upon LPS + nigericin treatment for 5 min. Fractions were analyzed by SDS-PAGE and immunoblot as indicated (n=1; pilot fractionation experiment).

**Figure S6**: Graphical summary illustrating multiple roles of BTK as NLRP3 regulator.

**Table S1: Peptides used in this study.**

| Nr. | Contained tyrosine(s) | Sequence | Modifications | Use in Fig. | Manufacturer |
|---|---|---|---|---|---|
| | | Human NLRP3 | | | |
| 1 | Y84 | AINRRDLYEKAKRDE | | S3 | In house |
| 2 | Y123 | EWMGLLEYLSRISIC | | S3 | In house |
| 3 | Y136, Y140, Y143 | ICKMKKDYRKKYRKY | | S3 | In house |
| 4 | Y136, Y140, Y143 | KKDYRKKYRKYVRSR | | F2, F3 | In house |
| 5 | Y136, Y140, Y143 | YRKKYRKYVRSRFQC | | S3 | In house |
| 6 | Y136 | KKDYRKKFRKFVRSR | Y140F, Y143F | F2 | In house |
| 7 | Y140 | ICKMKKDFRKKYRKF | Y136F, Y143F | F2 | In house |
| 8 | Y143 | FRKKFRKYVRSRFQC | Y136F, Y140F | F2 | In house |
| 9 | Y168 | SVSLNKRYTRLRLIK | | F3, S3 | In house |
| 10 | Y249 | DWASGTLYQDRFDYL | | S3 | In house |
| 11 | Y255 | LYQDRFDYLFYIHCR | | S3 | In house |
| 12 | Y258 | DRFDYLFYIHCREVS | | S3 | In house |
| 13 | Y381 | SEAKRKEYFFKYFSD | | S3 | In house |
| 14 | Y385 | RKEYFFKYFSDEAQA | | S3 | In house |
| 15 | Y443 | SKTTTAVYVFFLSSL | | S3 | In house |
| 16 | Y518 | EVDCEKFYSFIHMTF | | S3 | In house |
| 17 | Y533, Y534 | QEFFAAMYYLLEEEK | | S3 | In house |
| 18 | Y136, Y140, Y143 | KKDFRKKFRKFVRSR | Y136F, Y140F, Y143F | F2 | In house |
| 19 | Y168 | SVSLNKRFTRLRLIK | Y168F | F2 | In house |
| 20 | Y136, Y140, Y143 | KKDpYRKKpYRKpYVRSR | Phospho-Y | F3 | In house |
| | | Murine NLRP3 | | | |
| 21 | Y132 | ICKKKKDYCKMFRRH | Y136F | S3 | In house |
| 22 | Y136 | KKDFCKMYRRHVRSR | Y132F | S3 | In house |
| 23 | Y144 | RHVRSRFYSIKDRNA | | S3 | In house |
| 24 | Y164 | SVDLNSRYTQLQLVK | | S3 | In house |
| 25 | Y132, Y136 | ICKKKKDYCKMYRRH | | F3 | In house |
| 26 | Y132, Y136 | ICKKKKDpYCKMpYRRH | Phospho-Y | F3 | In house |

603 **Table S2: Antibodies used in this study.**

| Specificity | Manufacturer | Cat. Nr. |
|---|---|---|
| mNLRP3 | Adipogen | AG-20B-0014-C100 |
| hNLRP3 | CST | #15101 |
| hBTK | BD | 611117 |
| mBTK | CST | #8547 |
| HA | CST | #3724 |
| Flag | Sigma-Aldrich | F1804 |
| p-Y | CST | #8954 |
| ASC | CST | #67824 |
| hIL-1β | R&D Systems | MAB601 |
| mIL-1β | CST | #12242 |
| mCaspase-1 | CST | #3866 |
| GAPDH | Thermo-Fisher | **#** MA5-15738 |
| Citrate synthetase | GeneTex | GTX110624 |
| Anti-Mouse IgG (H+L) HRP conjugate | Promega | W4021 |
| Anti-Rabbit IgG (H+L) HRP conjugate | Vector | PI-1000 |
| VeriBlot for IP Detection Reagent (HRP) | Abcam | Ab131366 |
| Anti-Flag® M2-Peroxidase (HRP) | Sigma-Aldrich | A8592 |

604

Figure 1

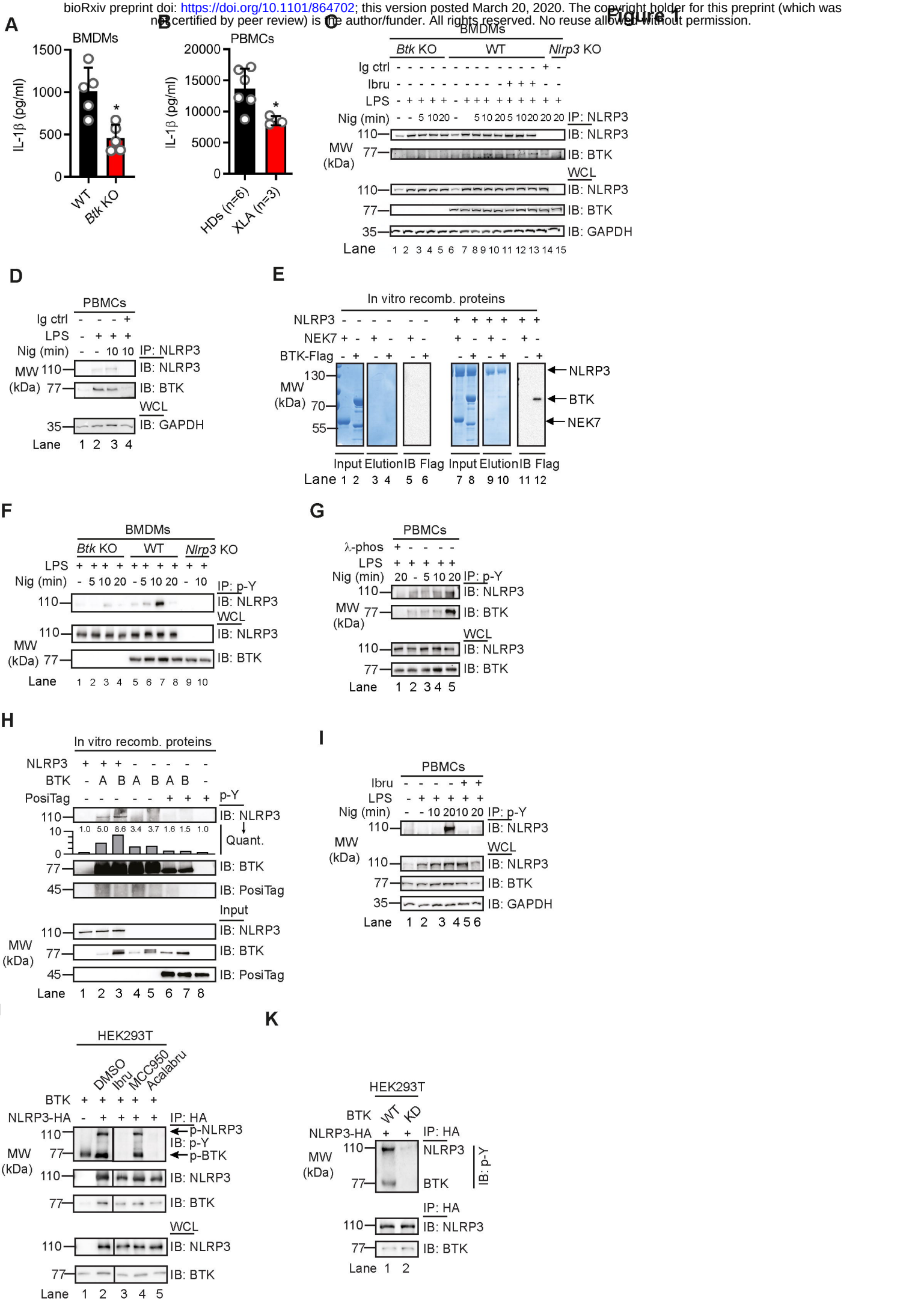

Figure 2

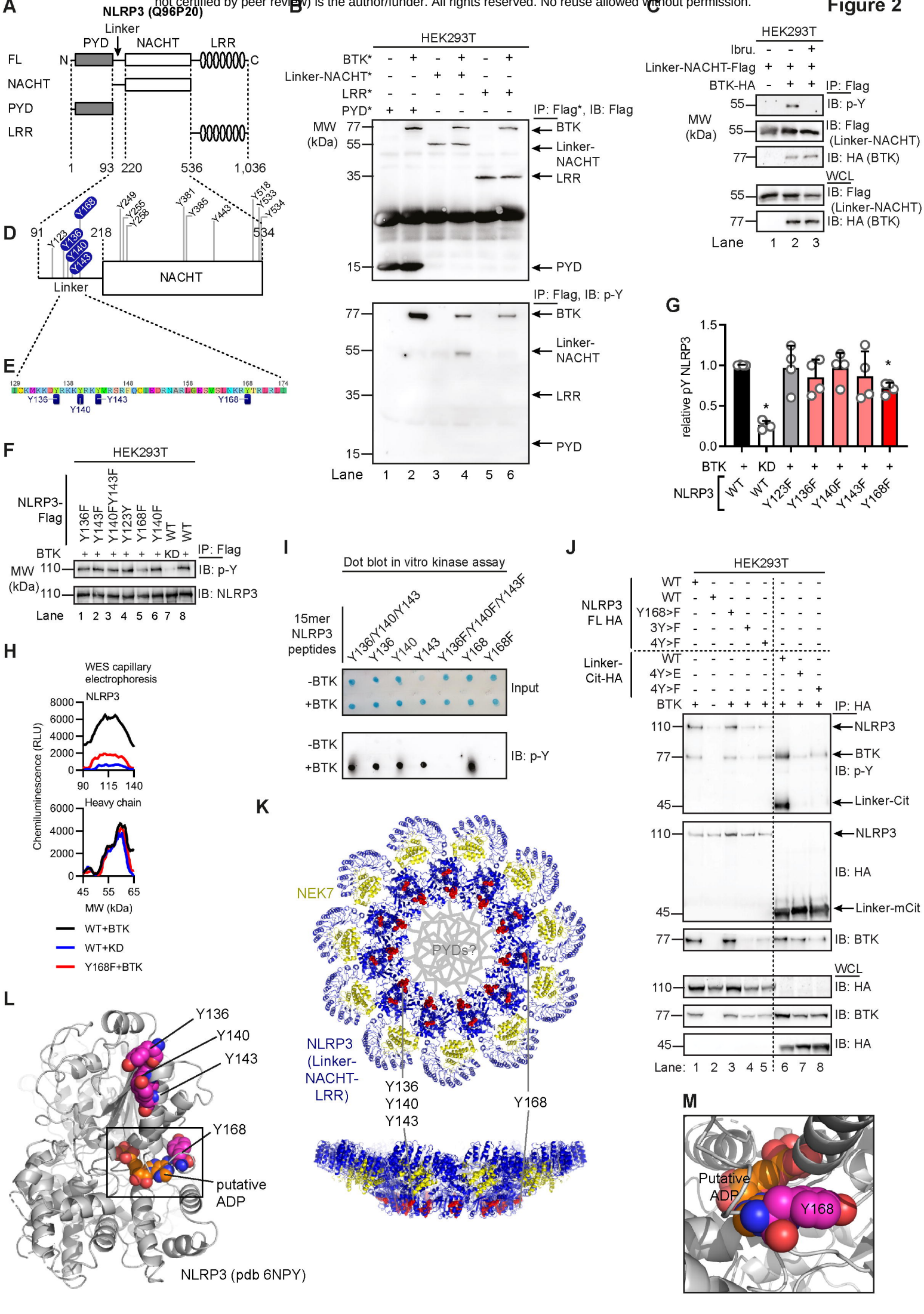

Figure 3

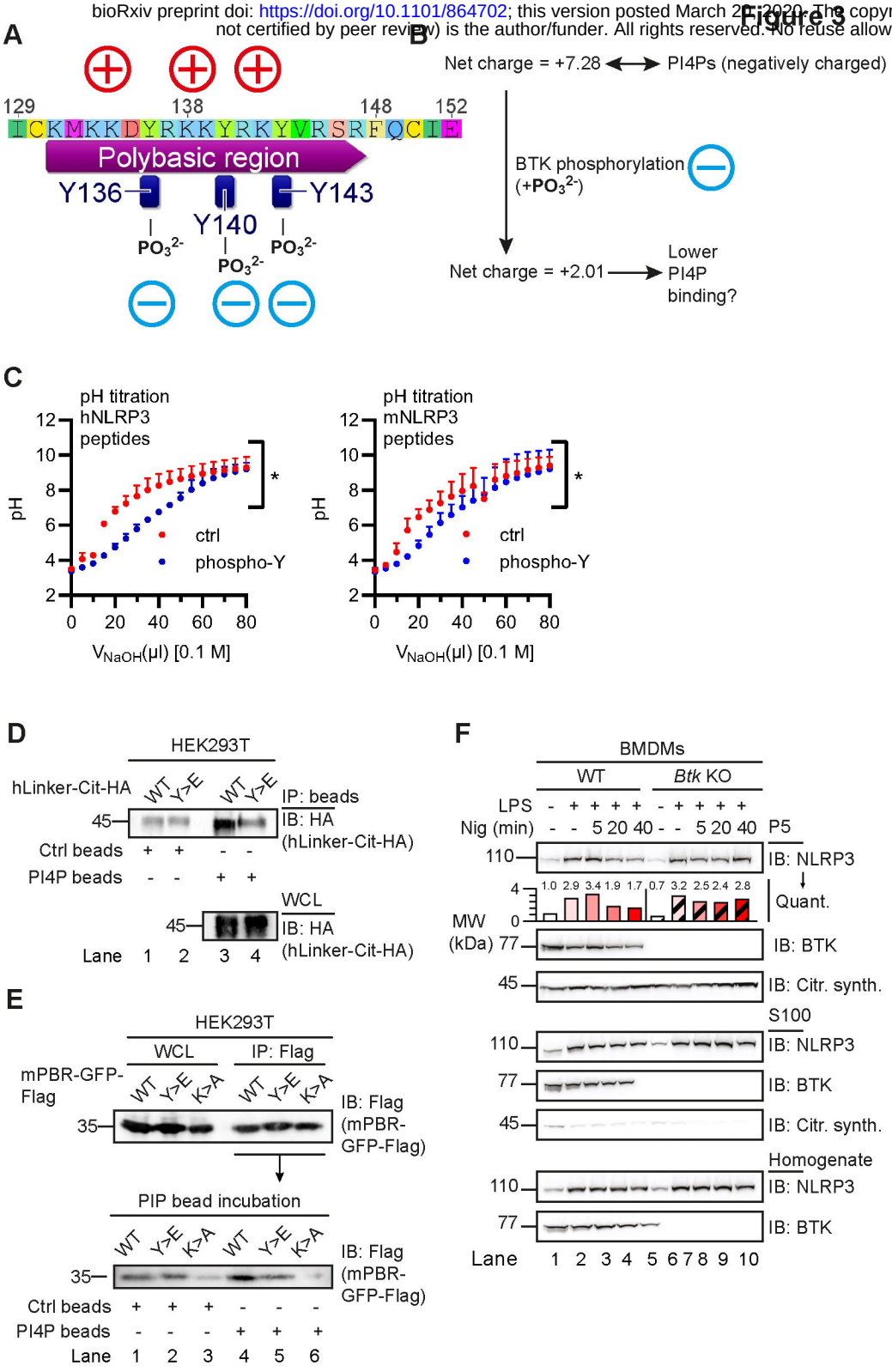

# Figure 4